Surf. Sci. **392,** 69 (1997)

The Structure of Silicon Surfaces from (001) to (111)

A. A. Baski [a], S. C. Erwin [b], and L. J. Whitman [b]

[a] *Physics Department, Virginia Commonwealth University, Richmond, VA 23284*

[b] *Naval Research Laboratory, Washington, DC 20375*

Abstract

We describe the structure of silicon surfaces oriented between (001) and (111) as determined by scanning tunneling microscopy (STM) and first-principles, total-energy calculations. In addition to reviewing and reproducing the structures reported for the few surfaces previously studied, we describe a number of additional surfaces in order to provide a complete overview of the (001)-to-(111) surface morphology. As the sample orientation is tilted from (001) to (111) ($\theta = 0°$ to 54.7°), the surface morphology varies as follows: 1) Si(001) to Si(114): (001)–like surfaces composed of dimers separated by steps (both rebonded and non-rebonded); 2) Si(114) to Si(113): mesoscale sawtooth facets composed of the stable (114)–2×1 and (113)–3×2 planes; 3) Si(113) to Si(5 5 12): mesofacets composed of (113)–3×2 and (5 5 12)–like planes; 4) Si(5 5 12) to ~Si(223): nanoscale sawtooth facets composed of (5 5 12)–like and unit-cell-wide (111)–7×7 planes; and 5) ~Si(223) to Si(111): (111)–7×7 terraces separated primarily by single- and triple-layer steps. The change in the surface morphology is accompanied by a change in the composition of surface structural units, progressing from (001)–like structures (e.g. dimers, rebonded steps, and tetramers) to (111)–like structures (π-bonded chains, adatoms, and dimer-chain walls). The resultant morphology is a delicate balance between the reduction of dangling bond density achieved by the formation of these structural units, and the resulting surface stress associated with their unusual bond angles and bond lengths.

Keywords: Silicon, Surface structure, Morphology, Reconstruction, High-index surfaces, Scanning tunneling microscopy

PACS Codes: 68.35.Bs, 61.16.Ch, 73.61.Cw

1. Introduction

No comprehensive surface energy diagram yet exists for silicon. As a consequence, the surface structure of a Si sample cut to any arbitrary orientation is usually not known. In addition to the fundamental importance of understanding the structure and stability of Si surfaces, this knowledge is of potential utility in the development of surface-dependent technologies such as heteroepitaxy for electronic devices [1] and fabrication of micro-electromechanical systems (MEMS) [2]. In the range of orientations between (001) and (111) the morphology of a number of surfaces have been determined using diffraction and microscopy techniques. Based on such techniques, atomic models have been proposed for the most well-known stable orientations [3], (001), (111) and (113) [4-7], as well as for two recently discovered stable planar surfaces, Si(114) and Si(5 5 12) (see Fig. 1) [8,9]. Away from these orientations, a number of different surface morphologies are known to exist, ranging from simple terrace-plus-step distributions to more dramatic sawtooth-like faceted structures.

In this study we present a comprehensive overview of silicon surface morphology from (001) to (111) as observed with scanning tunneling microscopy (STM) at room temperature. A diagram summarizing our results is shown in Fig. 2. The solid lines indicate orientations that form stable planar surfaces: (001), (114), (113), (5 5 12), and (111). Adjacent to each stable orientation is an atomic-resolution STM image of the reconstructed surface with its unit cell outlined. Vicinal Si surfaces with orientations close to the low index (001) and (111) planes have already been extensively investigated. As expected, Si(001) surfaces tilted only a few degrees toward (111) are composed of (2×1)-reconstructed (001) terraces separated by single-layer steps [10]. At higher tilt angles ($\theta = 2$–$5°$), double-layer steps with rebonded step edges become energetically favorable, as previously observed by Griffith *et al.* [11,12] and Swartzentruber *et al.* [13]. To date there have been very few STM studies of vicinal Si(001) surfaces with tilts > 6°. Recently, Hanbücken *et al.* examined concave-shaped Si(001) substrates having local orientations tilted as much as ≈12° [14]. They observed regions with local (119)- and (117)-orientations composed of (001) terraces separated by rebonded double-layer steps. In this work, we present STM studies of flat substrates within this range of orientations. We also find that surfaces with $\theta < 12°$ consist of (001) terraces separated by rebonded steps; however, surfaces at higher tilt angles ($\theta \geq 12°$) include both rebonded and *non-rebonded* steps. Our

previous studies of the stable Si(114)–2×1 surface (θ = 19.5°) demonstrated that both types of step edges also occur on this surface.

Beyond (114), the (001)-terrace-plus-step morphology breaks down and the surfaces become unstable with respect to faceting. Between (114) and (5 5 12), surfaces rearrange to form sawtooth-like *mesoscale* facets (50–100 nm wide) composed of the two nearest stable orientations: (114) and (113), or (113) and (5 5 12). This mesofaceting behavior has been previously observed by Suzuki *et al.* using reflection electron microscopy (REM) [15,16], and Song *et al.* using x-ray scattering and *ex-situ* atomic force microscopy [17,18]. In this study we describe these faceted surfaces, as well as the stable (5 5 12)–2×1 surface [9], as observed *in situ* with atomic-resolution STM. At orientations between (5 5 12) and ~(223), the surfaces are also unstable and rearrange to form sawtooth facets. As we reported in an earlier study [19], such surfaces form smaller *nanoscale* facets (~10 nm wide) composed of (111) and (5 5 12)–like nanoterraces. Finally, surfaces orientated between ~(223) and (111) rearrange to form (111)–7×7 terraces separated by single- and triple-layer steps, as previously established by Williams and coworkers [20,21].

We find that all silicon surfaces between (001) and (111) can generally be assembled from a few simple structural units: dimers, rebonded steps, tetramers, and π-bonded chains. These structures make two (related) contributions to the surface energy: (1) they reduce the density of dangling bonds, and (2) they contribute to the net surface stress tensor. Therefore, on any given surface the arrangement of such structures is a delicate energy balance between the elimination of dangling bonds and the minimization of surface stress. In this paper we discuss how the surface morphology varies from Si(001) to Si(111) as a consequence of these two competing principles.

2. Experiment

The experiments were performed in ultra-high vacuum (UHV) using Si wafers cut to within 0.5° of their nominal orientation. The samples were pre-cleaned in a boiling 1:3 solution of H_2O_2 and H_2SO_4, rinsed in distilled water, and then blown dry with nitrogen. Each sample was then mounted onto a button heater in UHV, degassed at 600 °C for 1 h, and then flashed to ≈1150 °C for 60 s (pressure ≤ 2×10^{-9} Torr). It is important to note that because the wafers were heated indirectly, the observed surface morphologies were not influenced by any electromigration

effects [17]. After cleaning, the samples were slowly cooled (≈ 2 °C/s) to room temperature. Atomic-resolution STM images of both the empty and filled electronic states were then acquired with a constant current of 0.1–0.3 nA and bias voltages between 1.0 and 2.5 V. All images presented here are topographs of the filled states unless otherwise noted. It is assumed that the observed morphology on each sample represents the equilibrium surface structure at room temperature.

3. Results

3.1 The family of (001)–like surfaces

It is well known that on the 2×1-reconstructed Si(001) surface the atoms pair up to form rows of dimers, thereby halving the density of dangling bonds. On surfaces vicinal to (001) the dimer rows form terraces having two possible orientations, with the dimer axis either perpendicular (type A) or parallel (type B) to the step at its upper edge [22]. For (001) surfaces tilted only a few degrees towards (111), both orientations of dimerized (001) terraces occur, separated by single-layer-height steps [10]. At higher tilt angles (≈ 4–5°), however, the surface consists primarily of B-type terraces separated by double-layer (type D_B) steps. This B-type terrace-plus-step morphology will be the focus of our discussion.

At a D_B step edge, the density of dangling bonds can be reduced by incorporating an extra row of atoms along the step, forming a *rebonded* step. Such a step was shown theoretically by Chadi to lower the total energy [22], and has been observed experimentally in a number of STM investigations [8,11-14]. Although an isolated rebonded step lowers the total energy, it introduces tensile surface stress perpendicular to the step edge. For periodic step arrays (e.g. vicinals), this stress becomes significant at higher tilt angles. In this study, we have observed that *non*-rebonded D_B steps (i.e. steps without an extra row of rebonding atoms) occur at orientations greater than $\theta \cong 12°$. To follow the evolution of the B-type terrace-plus-step morphology, we will now examine the following sequence of increasingly 'tilted' orientations**:** 1) Si(1 1 11) **(**$\theta = 7.3°$), 2) Si(119) ($\theta = 8.9°$), and 3) Si(117) ($\theta = 11.4°$).

3.1.1 Si(1 1 11) to Si(117)

The bulk-terminated (1 1 11) surface (Fig. 3a) can be considered a vicinal (001) surface composed of five (001) unit-cell-wide terraces separated by double-layer steps. If the surface were to maintain the terrace-plus-step morphology discussed above, it would reconstruct to form four-dimer-wide B-type (001) terraces separated by rebonded D_B steps (Figs. 3b,c). Note that the resulting (001) terraces would be only four dimers wide (not five), because the extra row of rebonding atoms prevents the row of atoms directly beneath the step from forming dimers. To investigate the agreement between this terrace-plus-rebonded step model and the actual reconstructed surface, we have obtained high-resolution STM images of the clean structure on a (1 1 11)-oriented sample. The images shown in Figs. 4a to 4c indicate an almost perfectly periodic array of row structures oriented along the $[\bar{1}10]$ direction. These rows have the expected $2a_o$ period (a_o = 0.38 nm) along the row direction and the (1 1 11) bulk periodicity (b_o = 2.1 nm) perpendicular to the rows. Although the surface is relatively well-ordered, defects such as isolated (1 1 13) unit cells (labeled 13 in Fig. 4b) and kinked steps occur, both due to a local misorientation of the sample. In addition, a low density of bright protrusions and dark defects can be seen on the surface, most likely as a result of isolated adsorbates and surface vacancies [14].

Using information from multiple-bias images and previous STM studies [8,14], the dominant features in these images can be identified as dimers and rebonded step edges. Within each (1 1 11)–2×1 unit cell, the four dimers on each (001) terrace appear as three bright maxima and one weak maximum, each labeled D in Fig. 4c. The adjacent maxima, labeled R, correspond to the rebonded D_B step edge, which usually has a $2a_o$ period along the row direction. Given that the rebonded step edge is expected to have only an a_o period, the observed doubling of the periodicity indicates that the rebonding atoms are tilting (or buckling) in and out of the plane, similar to the dimers on the upper terrace. In regions on the surface where the dimers do not appear strongly buckled, the adjacent rebonding atoms correspondingly demonstrate a much weaker $2a_o$ periodicity. It therefore appears that adjacent dimers influence the degree of buckling observed for the rebonded step edges, as previously discussed by Griffith *et al*. [12]. Note that the observation of occasional stretches with a_o periodicity along a row provides a simple method of identifying the row as a rebonded step (see, for example, the upper left of Fig. 4c).

As shown in Figs. 4d to 4f, the surface morphology of Si(119) ($\theta = 8.9°$) is very similar to that of Si(1 1 11). Again, there are row-like features with a $2a_o$ period along the row direction and a (119) bulk periodicity ($b_o = 1.75$ nm) perpendicular to the row direction. Given that the bulk-terminated (119) surface consists of four-unit-cell wide (001) terraces separated by double-layer steps, the reconstructed surface should contain three-dimer-wide (001) terraces separated by rebonded D_B steps. In Fig. 4f, these three dimers appear as two bright and one relatively weak maxima, whereas the rebonded D_B step edge appears as the fourth maxima. There is also a low density of (1 1 11) unit cells on this surface, indicating that the actual wafer orientation is tilted slightly away from (119) towards (1 1 11).

Lastly we examine Si(117) ($\theta = 11.4°$), which is expected to form two-dimer-wide B-type terraces separated by rebonded D_B steps. Atomic resolution images of Si(117) (Fig. 4i) show (117)-oriented terraces with the expected row periodicities [$2a_o$ (0.77 nm) × b_o (1.37 nm)]. Within each (117)–2×1 unit cell, the two adjacent dimers appear as an unresolved broad maxima (labeled DD), and the rebonded step edge corresponds to the smaller maxima. In contrast to (1 1 11) and (119), the (117)-oriented terraces are interrupted by unit cells of two other orientations: (119) and (115). On larger-scale images (Figs. 4g,h), these two orientations appear as rising and falling step edges of the (117) terraces. Each rising step edge corresponds to one unit cell of (119), whereas each falling step is two units of (115). Single unit cells of (115) are never observed. The frequent combination of two rising steps [(119)×2 units] followed by one falling step [(115)×2 units] maintains the overall local sample orientation [23].

3.1.2 Si(116) to Si(114)

As discussed above, surfaces with orientations from Si(1 1 11) to Si(117) behave essentially as expected, reconstructing to form (001)–2×1 terraces separated by rebonded D_B steps. The only deviation is the presence of paired (115) unit cells on the falling step edges found on Si(117). This deviation is actually the first indication that the simple terrace-plus-rebonded step morphology is modified at higher tilt angles. In fact, as we examine the next sequence of orientations, Si(116), Si(115), and Si(114), we will see that the paired (115) units represent the first local orientation to introduce a new atomic structure, *non*-rebonded steps,.

Si(116) is the first orientation presented here having an even index. Unlike odd-index surfaces, the bulk-terminated (116) surface is an *alternating* sequence of even (double) and odd (triple) width (001) terraces separated by double-layer steps. This sequence is equivalent to alternating bulk-terminated unit cells of the nearby odd-index planes, (117) and (115). As shown in Figs. 5a to 5c, the reconstructed (116) surface contains a non-periodic mixture of these two planes: short (117) terraces separated by paired (115) unit cells. A sequence of (115) and (117) units is labeled in Fig. 5c, with the boundaries defined by the rebonded step edges. Because the (115) unit cells occur only in pairs, the (117) units also appear in groups of two to three, although with no strict periodicity. In larger scale images, isolated steps infrequently appear which are steeper than neighboring (115) units (left and right sides of Fig. 5a). These 'steps' are actually single unit cells of yet another steeper orientation, (114).

Unlike the odd-index surfaces discussed up to now, Si(115) ($\theta = 15.8°$) has a complicated surface reconstruction that is not a simple extension of the periodic terrace-plus-rebonded step morphology (see Figs. 5d to 5f). Instead, the surface forms a quasiperiodic, sawtooth-like superstructure consisting of locally oriented (115), (117) and (114) unit cells (Fig. 5f). In larger scale STM images (Fig. 5d), the superstructure appears as prominent 'stripes' with a typical width of 5 nm. Each stripe is composed of the following subunits: a downward-sloping (114) unit cell, a planar region with paired (115) unit cells, and an upward-sloping (117) unit cell. This combination of subunits maintains the basal (115) orientation [24], resulting in a unit cell which is five times the bulk-terminated (115) period ($5 \times b_o = 5.0$ nm).

The atomic structures within the (117) subunit have already been discussed, so we will focus here on the isolated (115)–2×2 subunit. The bulk-terminated (115) surface (Fig. 6a) is composed of double-width (001) terraces separated by double-layer steps. If the simple terrace-plus-rebonded step morphology were applicable, then the reconstructed surface would consist of single dimers separated by rebonded D_B steps – but this structure is *not* observed. Instead, as Fig. 5f illustrates, the (115)-like structures on the surface reconstruct to form double-width (115) subunits composed of dimers, rebonded steps, and a new row structure (labeled T). This new structure appears as a row of block-like maxima with a weaker $2a_o$ periodicity. Such structures have been previously observed on other Si surfaces and are known as *tetramers* [7,8]: four-atom units consisting of a dimer adjacent to two *non-rebonded* step edge atoms. Figs. 6b and 6c

illustrate how these tetramers are incorporated into a reconstructed (115)–2×2 unit cell. Each 2×2 unit consists of a rebonded step, a dimer adjacent to a non-rebonded step (i.e. a tetramer), and a pair of dimers.

The presence of non-rebonded steps in the isolated Si(115)–2×2 subunits indicates that the simple terrace-plus-rebonded step morphology no longer applies to orientations tilted beyond ~11.4º [(117)], where these structures are first observed. This morphological change is most fully realized on Si(114) (Figs. 5g to 5i), which has a stable planar 2×1 reconstruction [8]. As indicated in Fig. 5i, the brightest maxima correspond to a rebonded step edge, the more variable maxima are a row of relatively buckled tetramers, and the less prominent maxima with a strict $2a_o$ spacing correspond to a single row of dimers. As illustrated in Figs. 7b and 7c, each reconstructed (114)–2×1 unit therefore consists of a rebonded step, a tetramer, and a *single* dimer [versus the pair of dimers in the (115)–2×2 unit cell]. Because (114) is an even-index surface, its bulk-terminated surface (Fig. 7a) is an alternating sequence of odd (single) and even (double) width (001) terraces separated by double-layer steps. However, unlike even-index surfaces closer to (001) [e.g. (116)], the reconstructed Si(114) surface is not composed of a mixture of unit cells of the nearby odd-index surfaces. Instead, it mimics the structure of the isolated (115)–2×2 unit cells, forming (001)–2×1 terraces (alternately single- and double-width), separated by alternately rebonded and non-rebonded D_B steps.

3.2. Si(114) to Si(5 5 12): mesoscale faceted surfaces

Whereas surfaces from (001) to (114) all share an (001)-terrace-plus-step morphology, this morphology breaks down for orientations steeper than (114) (19.5°). Surfaces between (114) and (113) are known to be unstable, restructuring into sawtooth-like facets composed of the nearby stable (114) and (113) surfaces [15,18]. Figs. 8a to 8c show images of such a faceted surface ($\theta = 21.5°$), with the (114) and (113) sides of the sawtooths labeled accordingly. Because this surface is oriented closer to (114) than to (113), the (114) sides are proportionally longer than the opposing (113) sides. Given the scale of these structures (50–100 nm wide by 1–2 nm high), we denote them *mesofacets*. Note that the mesofacets we observe are similar in size to those observed in earlier x-ray studies of extensively annealed samples [18], indicating that this is the equilibrium surface morphology.

As seen in the atomic-resolution image (Fig. 8c), the (113)–3×2 and (114)–2×1 reconstructions on the mesofacet surfaces are the same as on the corresponding planar samples. The bars marking the (114) units are aligned with the rebonded steps; the bars marking the (113) units are aligned with rows composed of alternating dimer and tetramer structures. Because the (113)–3×2 surface has already been extensively studied with STM and first-principles theoretical methods [7,25,26], we only briefly mention here that this surface is composed of the same elements found on the (001)–like surfaces: dimers, rebonded D_B steps and non-rebonded D_B steps (and possibly interstitials). One major difference, however, is the non-continuity of structures along the [$\bar{1}$10] direction. Rather than forming continuous rows of dimers or steps, as observed on the (001)–(114) family of surfaces, the (113)–3×2 reconstruction contains rows composed of alternating dimers and tetramers, resulting in a 3× periodicity along [$\bar{1}$10]. Si(113) is the *only* surface between (001) and (111) with a 3× reconstruction along the [$\bar{1}$10] row direction.

On the (113) faces of the mesofacets a large number of domain boundaries occur (short diagonal lines in Fig. 8b), suggesting that these defect structures are relatively low in energy. In contrast, steps are rarely observed, indicating that they are high energy defects. The (114)–2×1 reconstruction behaves in the opposite manner, incorporating no domain boundaries except those introduced by the occasional presence of bunched steps (see top left of Fig. 8b). At the tops and bottoms of the sawtooths the transitions between the (113) and (114) facets are surprisingly abrupt, occurring within only one or two unit cells. Within the region at the top edge of the sawtooths, a new structure is sometimes observed that appears as four maxima in a "scalloped" shape (labeled s in Fig. 8c). At present, its atomic structure is not known.

Recently, it was discovered that another stable surface, Si(5 5 12)–2×1 (θ = 30.5°), exists tilted only 5.3° away from (113) towards (111) [9,16,17]. As is the case for orientations between (113) and (114), surfaces between (113) and (5 5 12) are unstable and facet to the nearby stable planes, in this case (113) and orientations close to (5 5 12) [16,17]. As shown in Figs. 8d to 8f, the dimensions of these sawtooth-like facets and the sharpness of the transition regions are similar to those of the (113)/(114) mesofacets. The (113) sides of the facets form the expected 3×2 reconstruction (Figs. 8e and 8f), whereas the opposite sides form a slight variation of the stable Si(5 5 12) surface structure, i.e. they are not exactly oriented to (5 5 12).

To understand why these planes are only (5 5 12)–like, we must briefly examine the (5 5 12) surface itself. Fig. 9a shows the bulk-terminated (5 5 12) unit cell, which can be viewed as a combination of two (337) unit cells and a single (225) unit cell. As will be discussed below, the two (337) units (on the right and left) have distinctly different structures on the actual reconstructed (5 5 12) surface (Fig. 9c). In addition, (337) unit cells like those on the right in Fig. 9c are always observed paired with a (225) unit, a combination equivalent to a unit cell of (7 7 17). A reconstructed (5 5 12) surface therefore consists of an equal number of (7 7 17) and 'left-side' (337) units. Referring back to the mesofaceted images of Fig. 8f, we observe that there are nearly twice as many (7 7 17) units on the longer sides of the facets as 'left side' (337) units. As a consequence, these planes have only a (5 5 12)–*like* orientation [the actual local orientation is (17 17 41), 0.1º up from (5 5 12)].

When a surface is oriented to within a few degrees of (5 5 12), extended terraces of the stable (5 5 12)–2×1 reconstruction occur (Figs. 8g to 8i). The reconstructed terraces consist of well-ordered rows oriented along $[\bar{1}10]$, with the bulk-terminated periodicity perpendicular to the row direction (b_o = 5.35 nm). Three types of row structures can be identified on the (5 5 12) terraces: I, II and III, as indicated in Figs. 8i and 9d. Their sequence from left to right within each (5 5 12) unit cell is: I + III = (337) subunit (on left), and I + III + II + I + II = (7 7 17) subunit. The most prominent type-I rows have a bulk-like a_O period along the $[\bar{1}10]$ row direction, whereas the type-II and type-III rows both have a $2a_O$ period. In addition to these row structures, defect structures are often observed on top of the type-III rows. They appear as a single maximum in filled-state images and two maxima in empty-state images, suggesting the presence of adsorbed dimers [27].

Based on a careful examination of dual-bias images, we have proposed a model of the (5 5 12)–2×1 surface which incorporates structural units known to exist on other stable Si surfaces [9]. As a starting point, Figs. 9a and 9b show side and top views of a bulk-terminated (5 5 12) surface, respectively (one unit cell wide by ten deep). In order to obtain the reconstructed surface shown in Fig. 9c, the atoms locally rearrange to halve the density of dangling bonds (a rearrangement of 68 surface atoms per 2×1 unit cell). To accomplish this, two double rows of atoms are first removed to expose the regions which form the type-III rows. It is assumed that any unremoved atoms pair up to form the adsorbed dimer defects which occur in these regions. The remaining surface atoms are then locally rearranged to form (001)–like

features, such as dimers (D) and tetramers (T), or (111)–like features, such as π-bonded chains incorporated into 6- or 7-membered rings (π6, π7).

To more clearly illustrate these structures, a detailed model of the (225) subunit is shown in Fig. 10. The left half of the (225) subunit is a (111) plane segment, which reconstructs to form the two types of π-bonded chains: π6 and π7. The π7 chains are like those that occur on the metastable Si(111)–2×1 reconstruction [28,29], so their occurrence is not surprising. To our knowledge, π6 chains have not been previously observed, but they appear to be stable in first-principles electronic-structure calculations of the relaxed surface [30]. The right half of the subunit is a stepped (001) plane segment, which forms dimers and tetramers like those found on (001)–like surfaces. The correlation between these atomic structures and the observed rows is as follows: row I = π6 chain; row II = tetramers; and row III = π7 chain + dimer row. When this proposed model is used in conjunction with first-principles, electronic-structure calculations to obtain simulated STM images, the agreement between theory and experiment is excellent [9].

3.3. Si(5 5 12) to Si(111): nanofaceted and stepped surfaces

In the range of orientations between (5 5 12) ($\theta = 30.5°$) and (111) ($\theta = 54.7°$), single or multiple unit cells of the well-known (111)–7×7 (or 5×5) reconstruction are always present. An empty-state STM image of the 7×7 reconstruction is shown in Fig. 1, where the observed maxima correspond to the top-layer adatoms of the widely accepted dimer-adatom-stacking-fault (DAS) model [5]. As reviewed in the Introduction, surfaces oriented between (5 5 12) and ~(223) ($\theta = 43.3°$) are unstable and rearrange to form nanoscale sawtooth facets (*nanofacets*) composed of (5 5 12)–like planes and (111)–7×7 (or 5×5) nanoterraces. Surfaces oriented closer to (111) ($\theta \cong 43°$+ to 55°) also form (111)–7×7 terraces, but they are instead separated by single- and triple-layer steps [20,21]. Fig. 11 shows images of two nanofaceted surfaces, Si(112) ($\theta = 35.3°$) and Si(335) ($\theta = 40.3°$), as well as a stepped surface tilted 5.5° away from Si(111) ($\theta = 49.2°$).

In the large-scale STM image of the Si(112) surface (Fig. 11a), the striped features oriented along [$\bar{1}$10] correspond to the sawtooth-like nanofacets. The higher resolution image shown in Fig. 11c illustrates the atomic features of one such nanofacet. On the shorter side of the facet (labeled '1'), the triangular arrangement of maxima corresponds to a unit-cell-wide (111)–7×7

plane. On the longer side, the row-like features indicate the boundaries of (337) and (7 7 17) unit cells. Because there are three to five (337) unit cells for every (7 7 17) unit [vs. the 1:1 ratio on Si(5 5 12)], this plane has only a (5 5 12)–*like* orientation. As the sample orientation is tilted further towards (111), the relative number of single-width (111)–7×7 planes increases while the opposing (5 5 12)–like planes become narrower. Figs. 11d to 11f show the Si(335) surface, where the nanofacets have narrowed to only ≈ 6 nm. In this case, the nanofacets are so narrow that the (5 5 12)–like planes only rarely accommodate the wider (7 7 17) unit cells. Instead, most nanofacets incorporate only a few (337) units, which are typically adjacent to a relatively disordered region at the tops of the nanofacets.

Beyond this range of orientations ($\theta = 43°$ to 54.7°), the morphology becomes that of stepped Si(111). These surfaces are known to form (111)–7×7 terraces separated by single– and triple–layer steps, with the fraction of triples decreasing with increasing angle [20,21]. Figs. 11g to 11i show STM images of such a surface oriented 5.5° from (111), or approximately midway in this range of orientations. The (111)–7×7 terraces are two or more unit cells wide, and are separated primarily by triple-layer steps (T1, T2) and an occasional single-layer step (S). Interestingly, there are two distinct types of triple-layer steps. The T1 steps appear relatively well ordered and are no wider than the adjacent 7×7 terraces. In contrast, the T2 steps are wider and appear much more disordered, oftentimes incorporating what appear to be adsorbed dimers at the upper step edge (appearing as two bright maxima in the empty-state image of Fig. 11i). The T2 steps apparently occur when adjacent terraces have widths not equal to integral units of the (111)–7×7 unit cell. The percentage of T2 steps may decrease when the surface is cooled significantly slower, but such steps are still observed on samples cooled at rates one to two orders of magnitude slower than those cooled here [21].

4. Discussion

The reconstruction of semiconductor surfaces is driven by a delicate energy balance between the elimination of dangling bonds and the minimization of surface stress. In the family of (001)-like surfaces, these two competing factors help to explain the change in surface morphology as the sample orientation increases from vicinal (001) up to (114). For orientations up to (117), the surface is composed of (001)–2×1 terraces separated exclusively by *rebonded* D_B steps. The

rebonded steps minimize the density of dangling bonds, but at the cost of introducing tensile stress perpendicular to the step edge. This stress can be elastically relieved across the relatively wide terraces found on surfaces oriented up to (117). For orientations beyond (117), however, the terraces are only one or two dimers wide, leading to the introduction of *non-rebonded* steps with lower stress. Both non-rebonded and rebonded steps are present on the reconstructed (116), (115), and (114) surfaces. The density of such steps on the (114)–2×1 surface is sufficiently high that the two types of steps periodically alternate on the surface, separated by only *single*-width (001)–2×1 terraces (i.e. single dimers). This alternation between rebonded and non-rebonded steps has been shown theoretically to minimize both the dangling bond density and surface stress, leading to a stable planar surface [8].

For orientations beyond (114), the terraces separating such alternating steps are less than a single dimer wide, making the terrace-plus-step morphology no longer viable. Instead, orientations up to (113) form sawtooth facets composed of the two nearest stable surfaces, (114)–2×1 and (113)–3×2. These sawtooth facets grow only to mesoscopic dimensions (50 to 100 nm), suggesting that some mechanism may limit their size. It was pointed out by Marchenko that the stability of a sawtooth faceted surface is determined by the sum of its strictional energy and the energy cost of forming facet edges [31]. The facet edges introduce force densities on the surface which are balanced by elastic relaxations on the facets [32]. It is this balance that apparently leads to a preferred facet size on these surfaces.

Beyond (113), the next stable planar surface is (5 5 12)–2×1. The stability of this surface is perhaps unexpected, given its extremely large unit cell. Our proposed structural model, however, allows a simple and intuitively appealing explanation, based on the importance of considering both surface dangling bonds and surface stress. The density of dangling bonds (dbs) on the (5 5 12)–2×1 surface is a preliminary indication of its stability: in our model the density is 0.058 dbs/Å^2, a value between that for Si(001)–2×1 (0.068 dbs/Å^2) and Si(111)–7×7 (0.030 dbs/Å^2, assuming π-bonding effectively halves the density). To gain more quantitative insight, we have used first-principles methods to compute the surface energies and surface stress tensors of the three subunits of the (5 5 12) unit cell [30]. The surface energies for the two (337) subunits and the (225) subunit are in the range of 99–101 meV/Å^2. Given that these values are larger than those for Si(001)–2×1 or Si(111)–2×1 (~85 and ~90 meV/Å^2, respectively), it is not surprising

that planar surfaces with (337) or (225) orientations are not observed. The underlying reason for the instability of these planes, as well as the explanation for the stability of (5 5 12), is found in their calculated surface stress tensors. For the tensor components normal to [$\bar{1}$10], we find that the two (337) subunits are under intrinsic compressive stress, whereas the (225) subunit is under tensile stress. These opposing subunit stresses largely cancel each other on the (5 5 12) surface, leading to a lower net surface energy and the resulting stability of this plane.

As we have shown, surfaces tilted away from (5 5 12) are unstable. The surfaces reconstruct into sawtooth-like facets composed of (5 5 12)–like planes and the next nearest stable surface, either (113) or (111). In the case of surfaces oriented between (5 5 12) and (113), the facets have mesoscopic dimensions similar to those observed in the range of orientations between (113) and (114). In the range of orientations between (5 5 12) and ~(223), however, the surface is composed of significantly narrower (5 5 12)–like and (111) facets. The size of these nanofacets is determined by the strong tendency to form exactly *single*-unit-cell wide (111)–7×7 planes: given that the surface orientation determines the relative proportions of the two sides of the sawtooth, a fixed length for the (111) plane leads to a fixed length for the opposing (5 5 12)–like side. An 'ideal' nanofacet on a surface such as Si(112) might consist of one (111)–7×7 unit cell opposed by a terrace composed of four (337) units and one (7 7 17) unit cell [i.e. this combination is exactly coincident with the (112) basal plane]. There is some variance to this structure, however, because the local orientation is not always precisely maintained, and other unit cells are occasionally present [e.g. (112) and (559)]. As a consequence, the nanofacets have only a quasiperiodic structure [19].

It is interesting to note the subtle change in reconstruction found on the (5 5 12)–like planes on both the meso- and nanofaceted surfaces. As mentioned earlier, there are equal numbers of (337) and (7 7 17) unit cells on the reconstructed (5 5 12)–2×1 surface. In the case of the mesofacets, there are more (7 7 17) than (337) units (see Figs. 8d–8f). This imbalance indicates that unit cells oriented closer to the basal plane are favored, i.e. on a surface with orientation $\theta = 26.7°$, (7 7 17) units ($\theta = 30.2°$, $\Delta = 3.5°$) are favored over (337) units ($\theta = 31.2°$, $\Delta = 4.5°$). The reverse situation occurs on the nanofaceted surfaces. For surfaces oriented between $\theta = 35°$ to 40° (see Figs. 11a–11f), the (337) units ($\Delta \geq 3.8°$) are very much favored over the (7 7 17) units ($\Delta \geq 4.8°$).

When the surface orientation reaches (335) ($\theta = 40.3°$), the (5 5 12)–like sides of the nanofacets are so short that only one or two (337) unit cells can be accommodated. In this study, we do not present data from nanofaceted surfaces tilted beyond (335). However, it is expected that a transition region of a few degrees occurs between those surfaces which can be categorized as nanofaceted and those which consist of (111) terraces separated by single– or triple–layer steps. Surfaces oriented close to Si(223) ($\theta = 43.3°$) have been examined in STM studies by a number of groups [21,33,34]. All groups observed (111)–7×7 terraces and step structures, but Berghaus *et al.* also observed row-like structures similar to the π-chains found within reconstructed (337) unit cells. The orientation for which this structure is no longer energetically favorable is therefore in the range from $\theta \approx 40°$ to 43°. Beyond this orientation ($\theta > 43°$), surfaces are simply composed of (111)–7×7 terraces separated by single- and triple-layer steps [20,21].

5. Conclusions

This work describes the myriad of morphologies occurring on silicon surfaces oriented between (001) and (111) in the framework of five regimes: (001) to (114) = (001) terraces plus steps; (114) to (113) = (114)/(113) mesofacets; (113) to (5 5 12) = (113)/(5 5 12)-like mesofacets; (5 5 12) to (223) = (5 5 12)-like/(111) nanofacets; and (223) to (111) = (111) terraces plus steps. The boundaries between all but the last two regimes are stable, planar reconstructions. These reconstructed surfaces are composed of a relatively small number of structural units – dimers, rebonded and non-rebonded steps, and π-bonded chains – that reduce the dangling bond density. However, the unusual bond lengths and bond angles required to form these surface structures inherently introduce surface stress. It is the balance between this surface stress and the reduced dangling bond density that leads to a local minimum in the surface energy for certain orientations and, therefore, to a stable planar reconstruction. For most other orientations this surface energy is minimized by forming facets of nearby stable planes. It is important to note that the surface energy can be easily altered by adsorbates, resulting in a large-scale restructuring of the surface [35,36]. Although we are making progress in developing a fundamental understanding of the structure of clean silicon surfaces, the extension of these ideas to adsorbate-covered surfaces is a much more difficult task. We expect that progress towards

this goal – important for both technical applications as well as fundamental science – will continue to require the close interplay of theory and experiment.

Acknowledgments

The authors thank Professors S. G. J. Mochrie and E. D. Williams for providing silicon samples. Computational work was supported by the Cornell Theory Center and by a grant of HPC time from the DoD Shared Resource Center MAUI. This work was funded by the Office of Naval Research and an NRL/NRC Postdoctoral Fellowship (A.A.B.).

References

[1] N. K. Dhar, C. E. C. Wood, A. Gray, H. Y. Wei, L. Salamanca-Riba and J. H. Dinan, J. Vac. Sci. Technol. B 14 (1996) 2366.

[2] D. L. Kendall, W. P. Eaton, R. Manginell and T. G. D. Jr., Opt. Eng. 33 (1994) 3578.

[3] Thermodynamically, a stable (or singular) surface represents a cusp in the Wulff surface energy plot. Experimentally, a wafer with such an orientation forms large, flat terraces of the basal plane after cleaning with standard procedures.

[4] R. Becker and R. Wolkow, in *Scanning Tunneling Microscopy*, edited by J. A. Stroscio and W. J. Kaiser (Academic Press, San Diego, CA, 1993) 149.

[5] K. Takayanagi, Y. Tanishiro, M. Takahashi and S. Takahashi, J. Vac. Sci. Technol. A 3 (1985) 1502.

[6] W. Ranke, Phys. Rev. B 41 (1990) 5243.

[7] J. Knall, J. B. Pethica, J. D. Todd and J. H. Wilson, Phys. Rev. Lett. 66 (1991) 1733.

[8] S. C. Erwin, A. A. Baski and L. J. Whitman, Phys. Rev. Lett. 77 (1996) 687.

[9] A. A. Baski, S. C. Erwin and L. J. Whitman, Science 269 (1995) 1556.

[10] H. J. W. Zandvliet and H. B. Elswijk, Mod. Phys. Lett. B 7 (1993) 1547.

[11] J. E. Griffith and G. P. Kochanski, Solid State and Materials Sciences 16 (1990) 255.

[12] J. E. Griffith, G. P. Kochanski, J. A. Kubby and P. E. Wierenga, J. Vac. Sci. Technol. A 7 (1989) 1914.

[13] B. S. Swartzentruber, N. Kitamura, M. G. Lagally and M. B. Webb, Phys. Rev. B 47 (1993) 13432.

[14] M. Hanbücken, B. Röttger and H. Neddermeyer, Surf. Sci. 331-333 (1995) 1028.

[15] T. Suzuki, Y. Tanishiro, H. Minoda, K. Yagi and M. Suzuki, Surf. Sci. 298 (1993) 473.

[16] T. Suzuki, H. Minoda, Y. Tanishiro and K. Yagi, Surf. Sci. 348 (1996) 335.

[17] S. Song, M. Yoon and S. G. J. Mochrie, Surf. Sci. 334 (1995) 153.

[18] S. Song and S. G. J. Mochrie, Phys. Rev. B 51 (1995) 10068.

[19] A. A. Baski and L. J. Whitman, Phys. Rev. Lett. 74 (1995) 956.

[20] J. Wei, X. S. Wang, J. L. Goldberg, N. C. Bartelt and E. D. Williams, Phys. Rev. Lett. 68 (1992) 3885.

[21] B. Li, Ph.D. thesis, University of Maryland (1993).

[22] D. J. Chadi, Phys. Rev. Lett. 59 (1987) 1691.

[23] Given that (119) = 4×(001) + 1 DL step and (115) = 2×(001) + 1 DL step, then 2×(119) + 2×(115) = 12×(001) + 4 DL steps = 4×(117), where (117) = 3×(001) + 1 DL step.

[24] Given that (117) = 3×(001) + 1 DL step and (114) = 3×(001) + 2 DL steps, then (117) + (114) = 6×(001) + 3 DL steps = 3×(115), where (115) = 2×(001) + 1 DL step. Because the superperiodic structure also includes two unit cells of (115), its period is equivalent to 5 unit cells of (115), or 5 nm.

[25] J. Dabrowski, H. J. Müssig and G. Wolff, Phys. Rev. Lett. 73 (1994) 1660.

[26] D. M. Bird, L. J. Clarke, R. D. King-Smith, M. C. Payne, I. Stich and A. P. Sutton, Phys. Rev. Lett. 69 (1992) 3785.

[27] P. J. Bedrossian, Phys. Rev. Lett. 74 (1995) 3648.

[28] R. M. Feenstra and J. A. Stroscio, Phys. Rev. Lett. 59 (1987) 2173.

[29] K. C. Pandey, Phys. Rev. Lett. 49 (1982) 223.

[30] S. C. Erwin, A. A. Baski and L. J. Whitman, to be published.

[31] V. I. Marchenko, Sov. Phys. JETP 54 (1981) 605.

[32] R. J. Phaneuf, N. C. Bartelt and E. D. Williams, Phys. Rev. Lett. 67 (1991) 2986.

[33] T. Suzuki, H. Minoda, Y. Tanishiro, K. Yagi, H. Kitada and N. Shimizu, Surf. Sci. 357 (1996) 73.

[34] T. Berghaus, A. Brodde, H. Neddermeyer and S. Tosch, J. Vac. Sci. Technol. A 6 (1988) 478.

[35] E. D. Williams and N. C. Bartelt, Science 251 (1991) 393.

[36] A. A. Baski and L. J. Whitman, J. Vac. Sci. Technol. B 14 (1996) 992.

Figure Captions

Fig. 1. Side view of the silicon crystal lattice between the (001) and (111) planes. The intersections of the lattice lines represent projections of atomic positions onto the {110} plane (the plane of the page). Single unit cells of a number of bulk-terminated orientations are marked with solid circles, and the corresponding angle θ and unit cell length (L) are listed in the adjacent table. Given a Miller index (hhk), $\tan\theta = \sqrt{2}h / k$.

Fig. 2. Diagram of the surface morphologies observed on silicon surfaces oriented between (001) and (111). The solid lines denote orientations with stable, planar reconstructions. STM images of these reconstructions are shown with their corresponding unit cells outlined [all images are of filled-states, except for the (111)-7×7]. The dashed lines denote the approximate orientations dividing the indicated structures.

Fig. 3. (a) Side view of a bulk-terminated Si(1 1 11) surface, where the dashed line indicates a five-unit-cell wide (001) terrace and 'DL' marks a double-layer step. (b) Side and (c) top views of a proposed model for the Si(1 1 11)–2×1 reconstructed surface (unit cell = 0.77 nm × 2.13 nm).

Fig. 4. Matrix of filled-state STM images where the column indicates the sample orientation: (a)–(c) Si(1 1 11); (d)–(f) Si(119); (g)–(i) Si(117), and the row indicates the square image size: (a),(d),(g) 120 nm; (b),(e),(h) 30 nm; (c),(f),(i) 10 nm. On the bottom row of atomic-resolution images, the unit cells on each surface are labeled [k = (11k), e.g. 9 = (119)], along with the periodic atomic structures (D = dimer and R = rebonded double-layer step edge).

Fig. 5. Filled-state STM images for sample orientations (a)–(c) Si(116), (d)–(f) Si(115), and (g)–(i) Si(114). The square images are: (a),(d),(g) 120 nm; (b),(e),(h) 30 nm; (c),(f),(i) 10 nm. The unit cells on each surface are labeled, k = (11k), along with the atomic structures (D = dimer, R = rebonded step edge, and T = tetramer). Note that the (115) unit cells only occur in pairs, denoted "2×(115)."

Fig. 6. (a) Side view of a bulk-terminated Si(115) surface, where dashed lines indicate double-width (001) terraces separated by double-layer steps (DL). (b) Side and (c) top views of a proposed model for a reconstructed Si(115)–2×2 unit cell (0.77 nm × 2.0 nm). Note that the combination of one dimer and two non-rebonded step-edge atoms is called a tetramer.

Fig. 7. (a) Side view of a bulk-terminated Si(114) surface, where dashed lines indicate single- and double-width (001) terraces separated by double-layer steps (DL). (b) Side and (c) top views of a proposed model for the Si(114)–2×1 reconstructed surface (unit cell = 0.77 nm × 1.63 nm).

Fig. 8. Filled-state STM images for sample orientations (a)–(c) Si(113) – 3.7°, (d)–(f) Si(113) + 1.5°, and (g)–(i) ≈Si(5 5 12). The square images are: (a),(d),(g) 372 nm; (b),(e),(h) 65 nm; (c) 14 nm; (f),(i) 30 nm. Images (b),(c),(e) and (f) have been high-pass filtered (flattened) in order to make the atomic-scale features more apparent. In the atomic-resolution images (bottom row), the unit cells on each surface are labeled as follows: 3 = (113), 4 = (114) and 17 = (7 7 17). The (337) units are indicated with arrows. In image (i) the three types of row structures associated with the Si(5 5 12)–2×1 reconstruction are marked as I, II, and III.

Fig. 9. (a) Side and (b) top views of a bulk-terminated Si(5 5 12) surface. Note that each (5 5 12) unit cell is equivalent to one unit cell of (337) plus one unit of (7 7 17). (c) Top view of a proposed model for the Si(5 5 12)–2×1 reconstructed surface (unit cell = 0.77 nm × 5.35 nm). The constituent atomic structures are labeled as follows: D = dimers, T = tetramers (dimer + non-rebonded step edge), and π6 (π7) = π-bonded chains atop 6-membered (7-membered) rings. (d) Rendered, filled-state STM image of the Si(5 5 12) surface. The three different row structures observed are denoted I, II, and III as indicated.

Fig. 10. (a) Side view of a bulk-terminated Si(225) surface. (b) Side and (c) top views of a proposed model for one reconstructed unit cell of Si(225)–2×1. All structures are labeled as in Fig. 9.

Fig. 11. Filled-state STM images for sample orientations (a)–(c) Si(112), (d)–(f) Si(335), and (g)–(i) Si(111) – 5.5°. The square images are: (a),(d),(g) 120 nm; (b),(e) 34 nm; (h) 33 nm; (c),(f),(i) 20 nm. All images except (i) are of the filled states, and all images except (a),(d) and (g) have been high-pass filtered (flattened) in order to make the atomic-scale features more apparent. In the atomic-resolution images (bottom row), the unit cells on each surface are labeled as follows: 1 = (111)–7×7, 17 = (7 7 17) and (337) = arrows. In image (i) a single-layer step (S) and two types of triple-layer steps (T1 and T2) are also indicated.

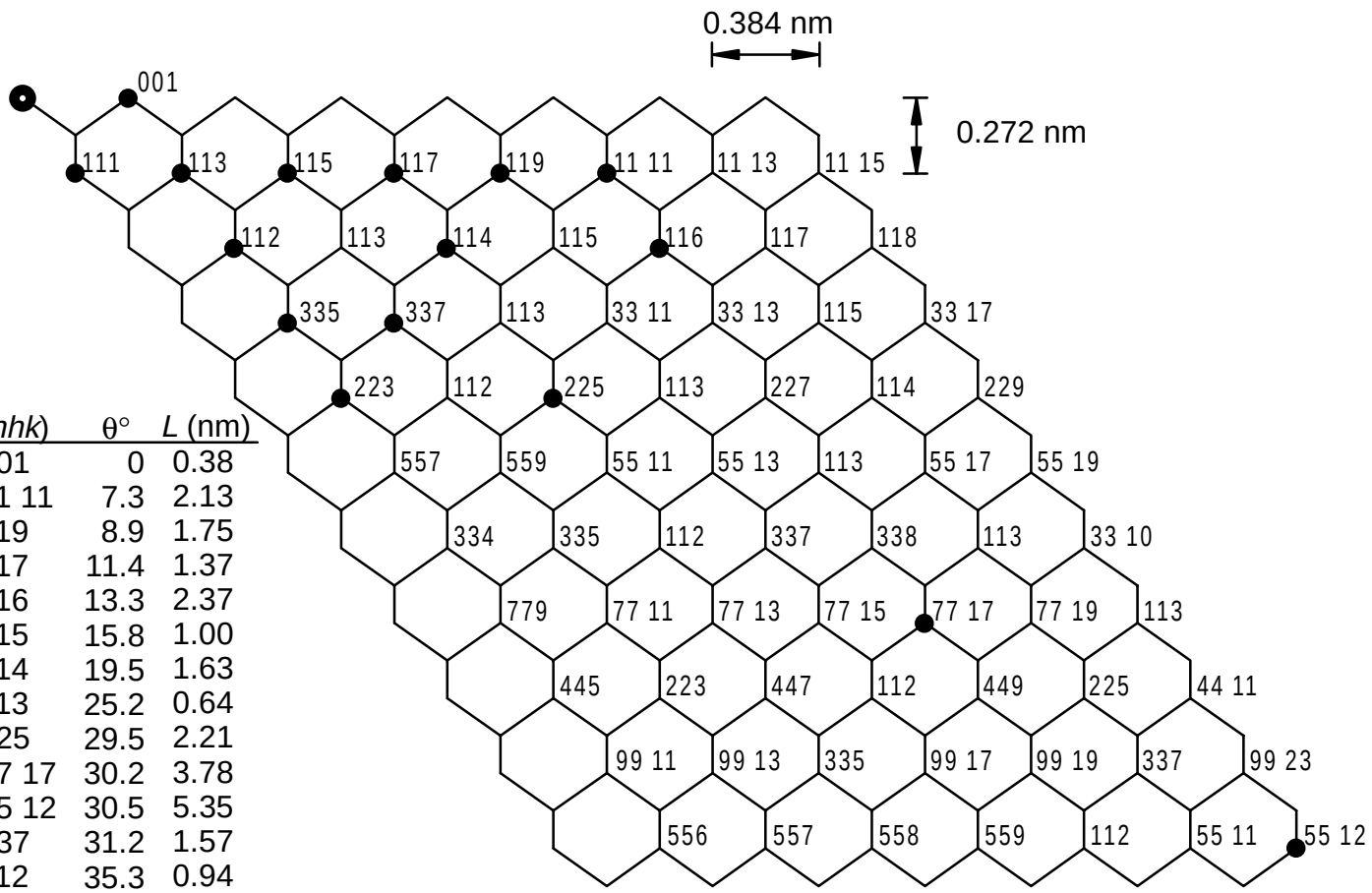

(*hhk*)	θ°	*L* (nm)
001	0	0.38
11 11	7.3	2.13
119	8.9	1.75
117	11.4	1.37
116	13.3	2.37
115	15.8	1.00
114	19.5	1.63
113	25.2	0.64
225	29.5	2.21
77 17	30.2	3.78
55 12	30.5	5.35
337	31.2	1.57
112	35.3	0.94
335	40.3	1.26
223	43.3	1.59
111	54.7	0.33

Figure 1

Baski *et al.*

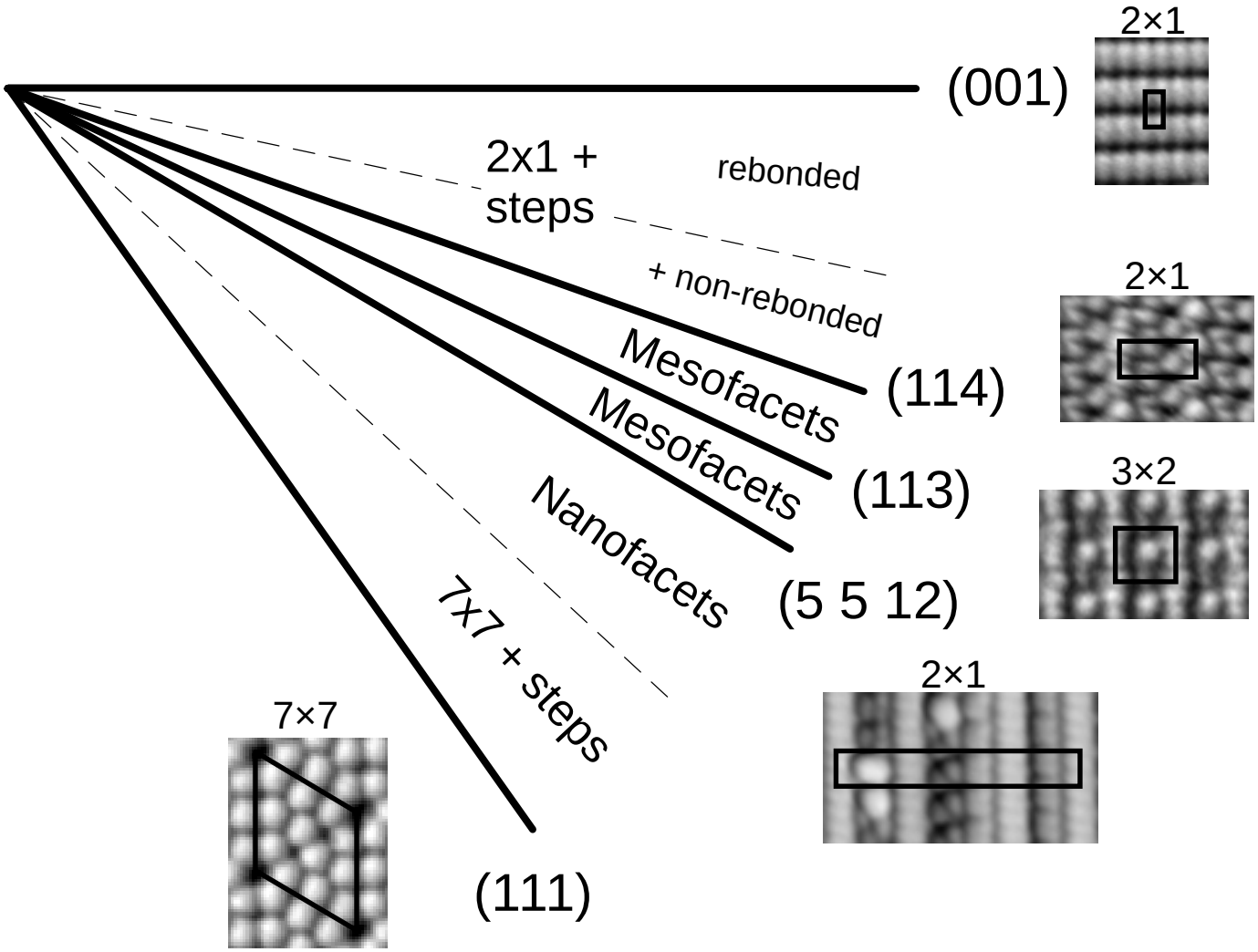

Figure 2

Baski *et al.*

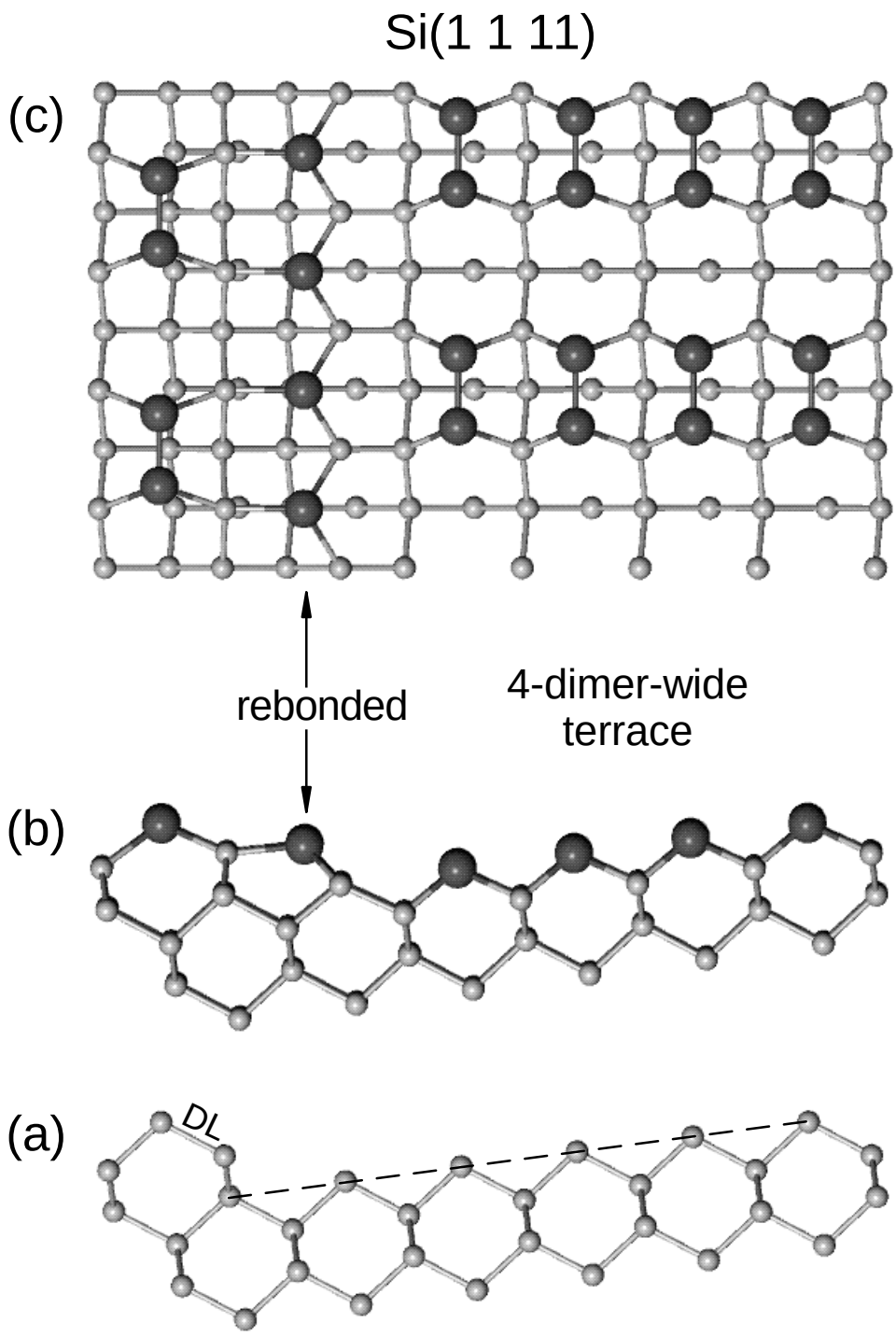

Figure 3

Baski *et al.*

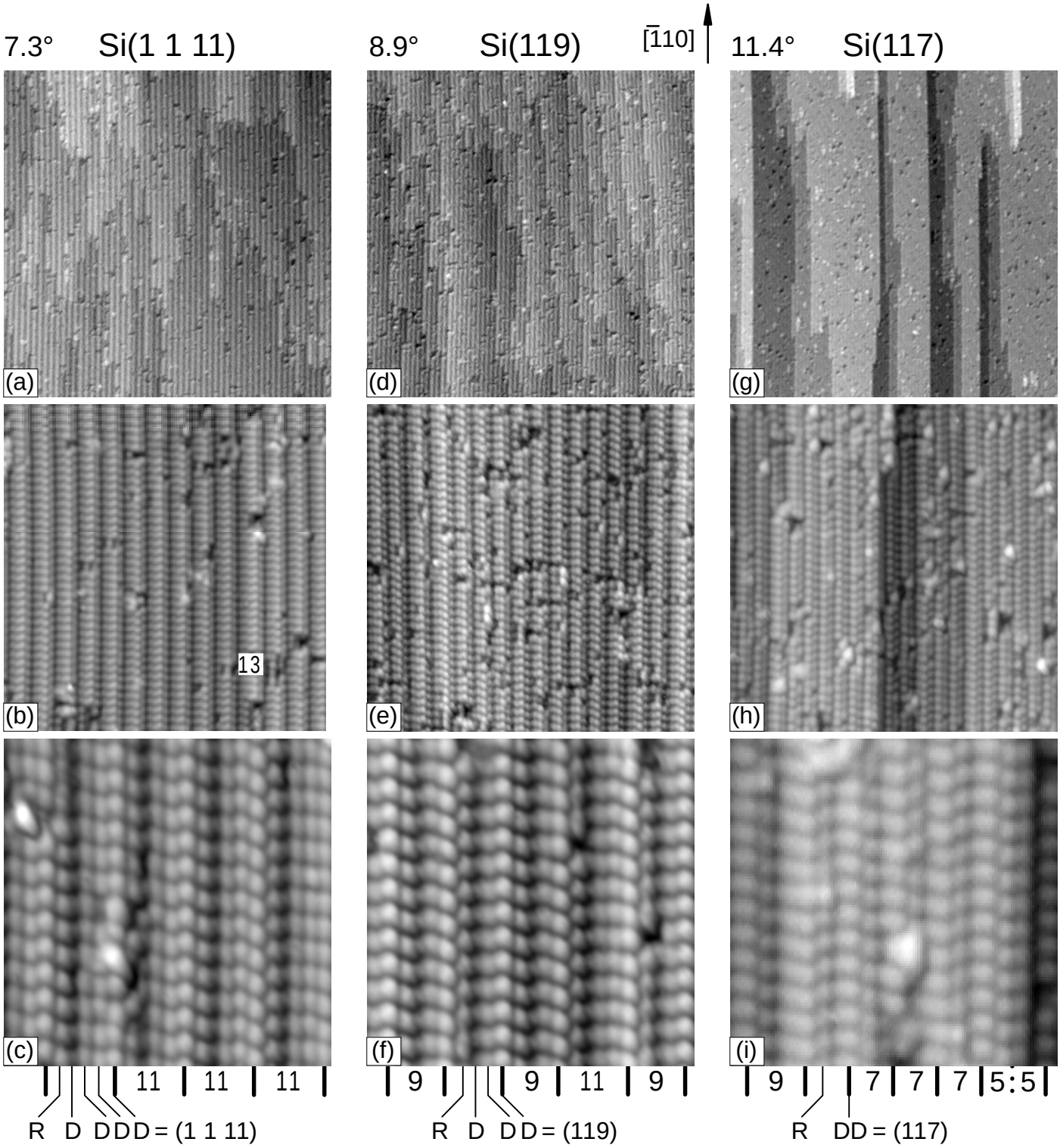

Figure 4

Baski *et al.*

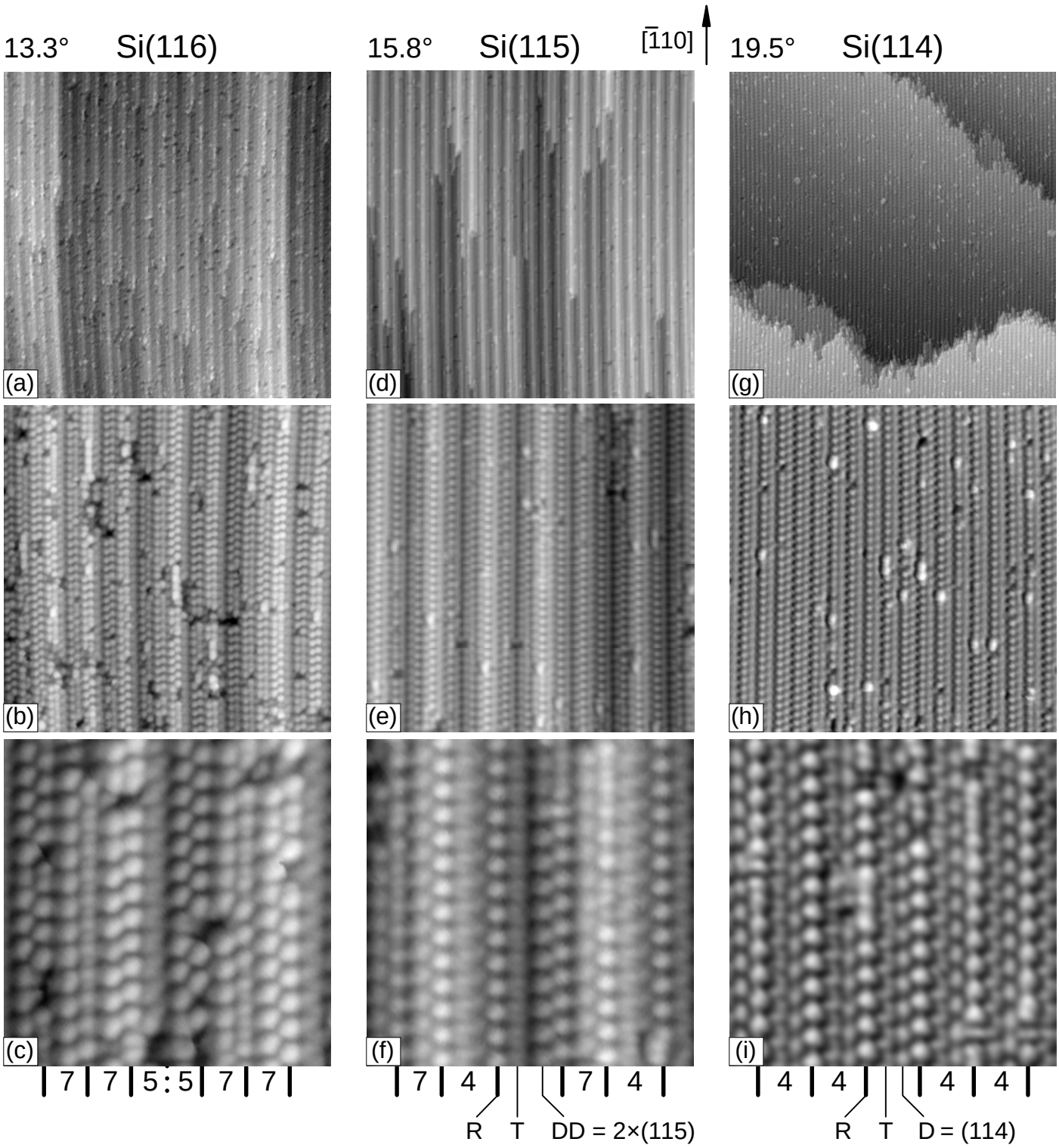

Figure 5

Baski *et al.*

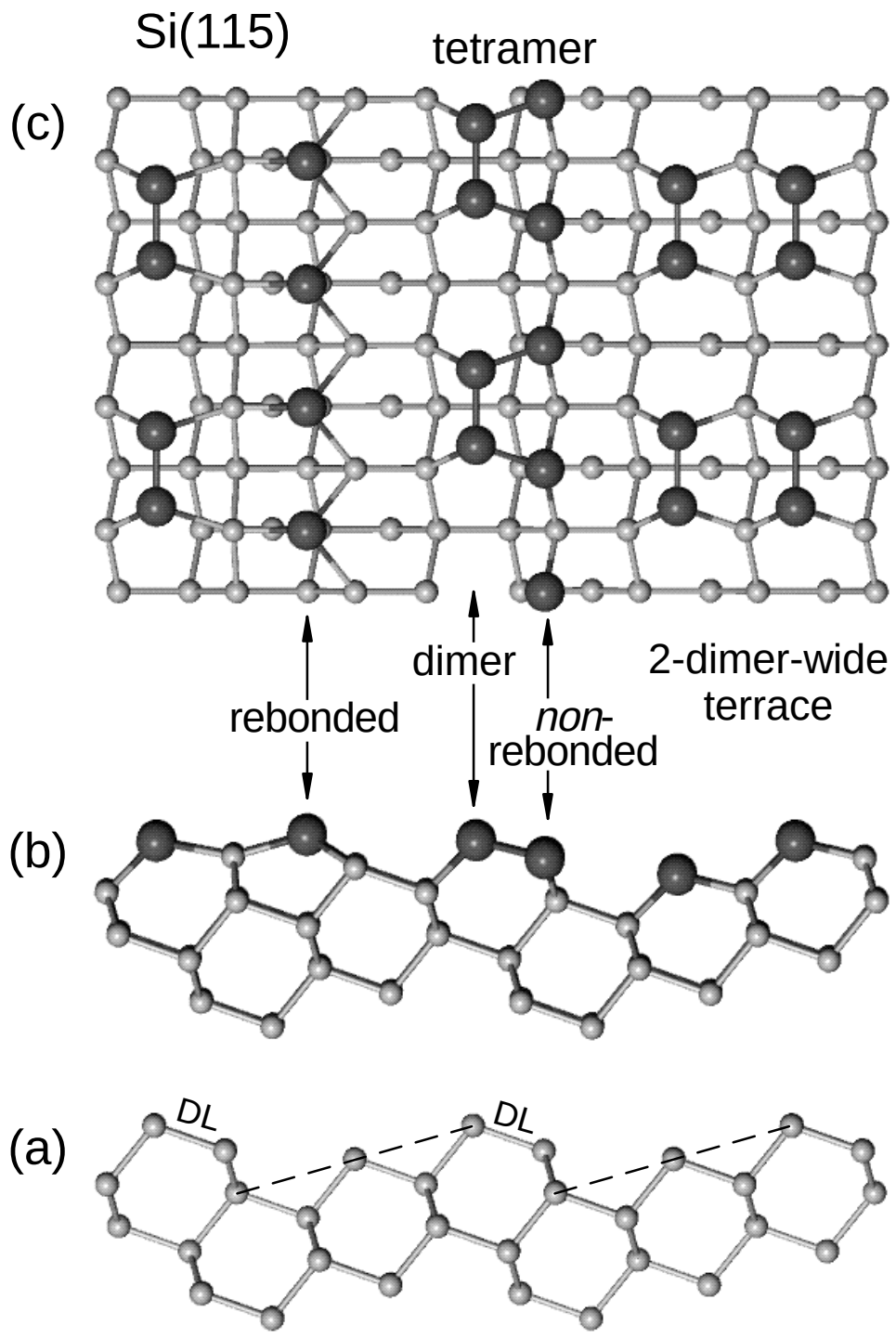

Figure 6

Baski *et al.*

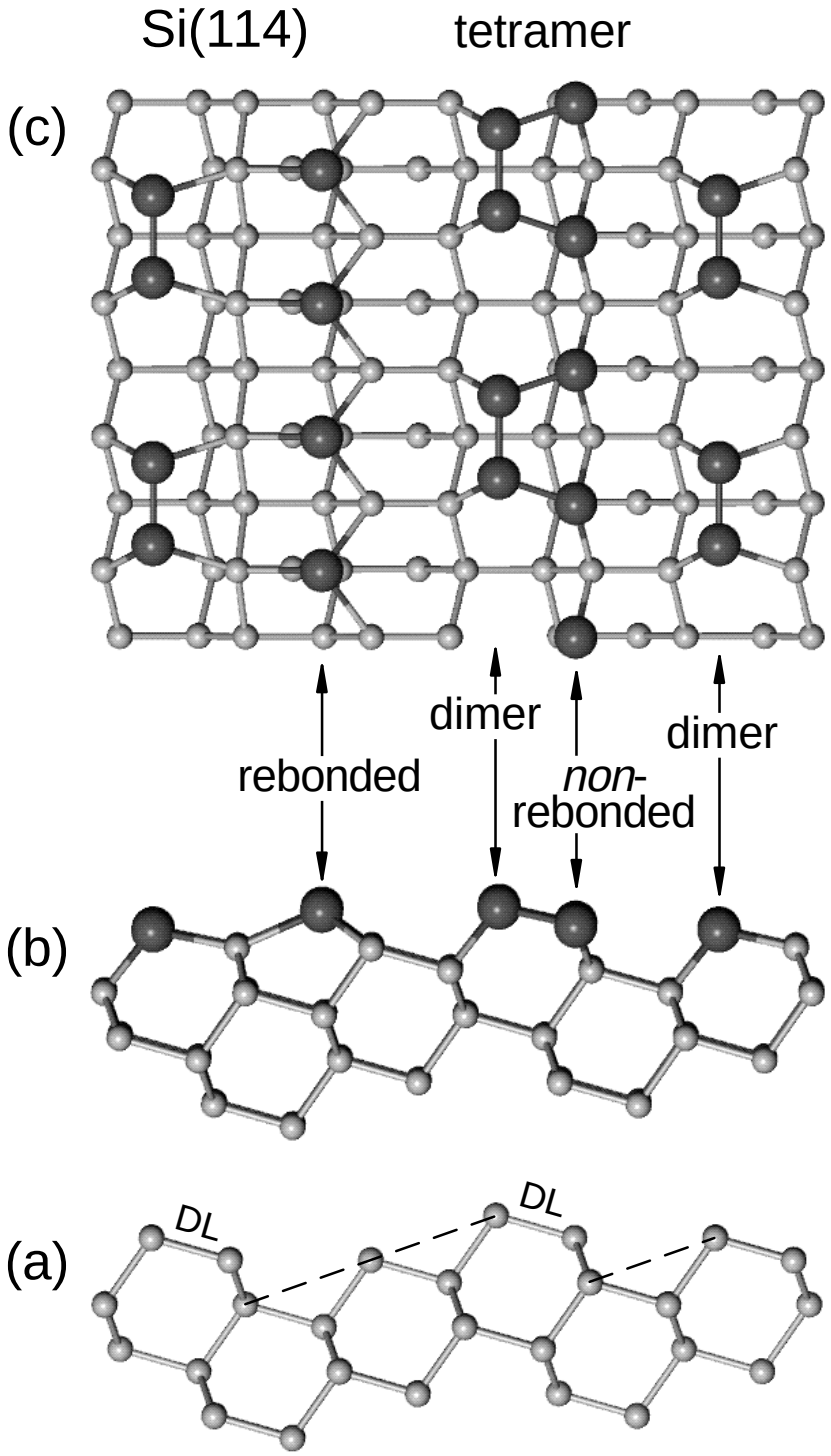

Figure 7

Baski *et al.*

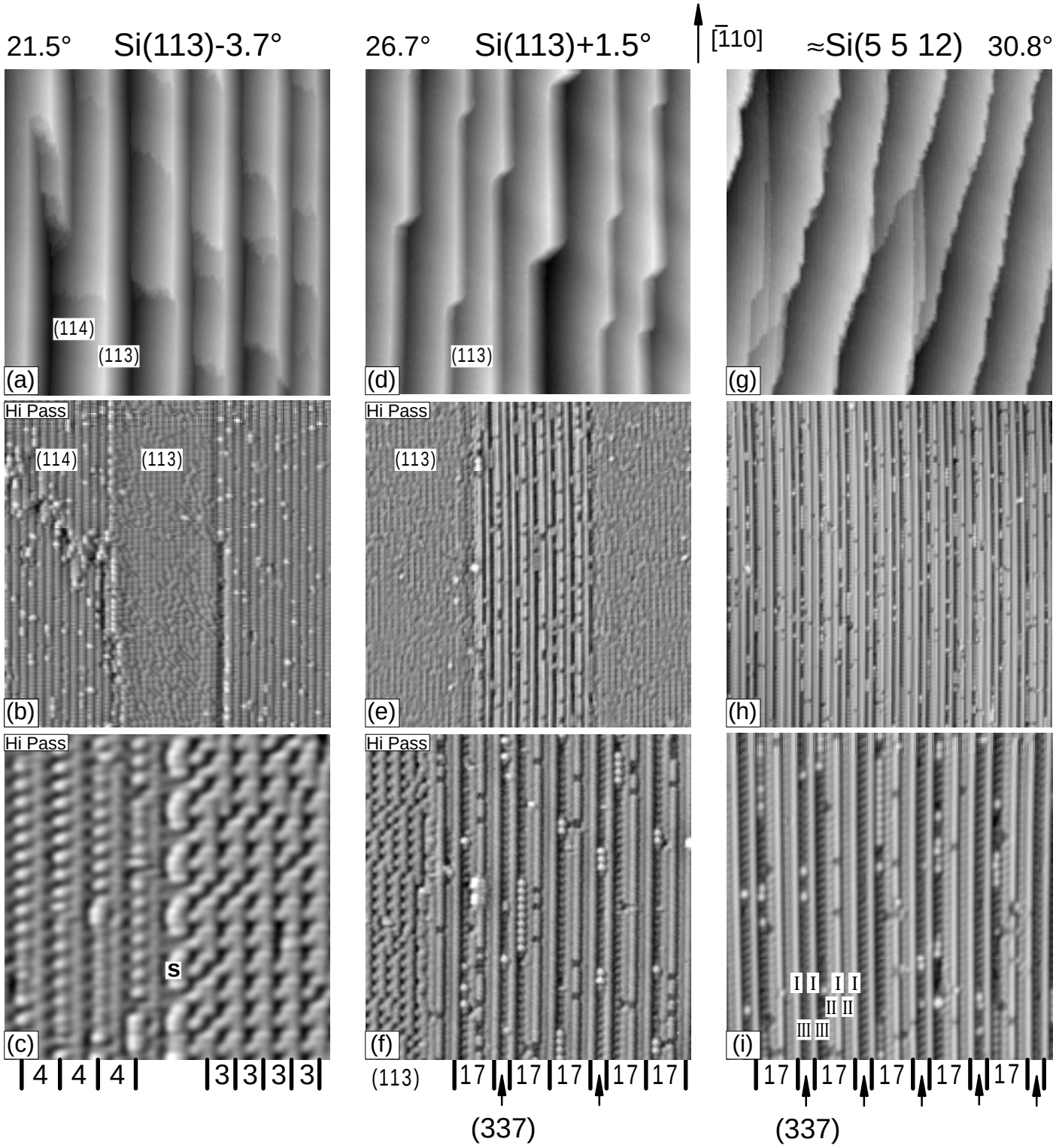

Figure 8

Baski *et al.*

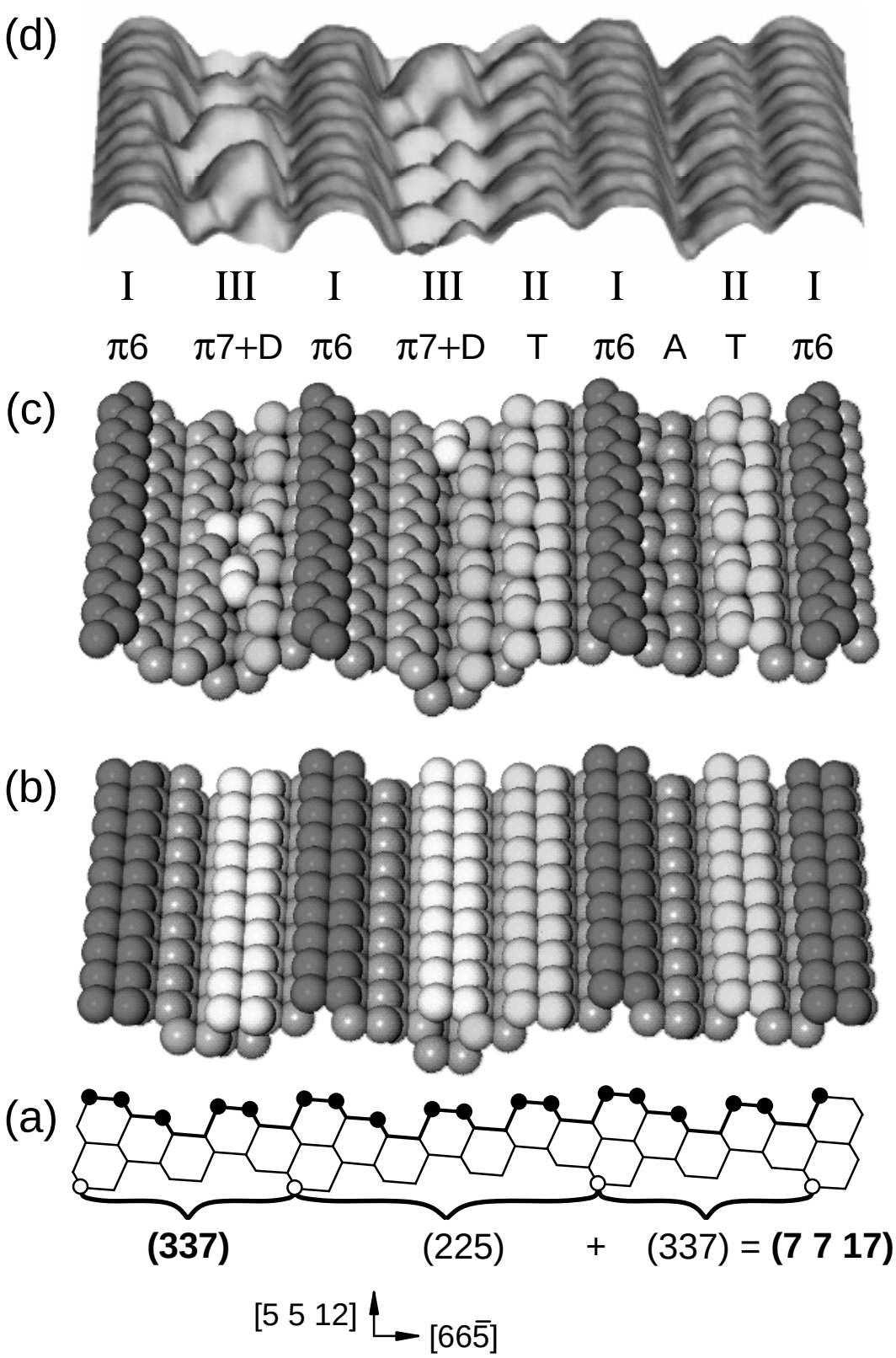

Figure 9

Baski *et al.*

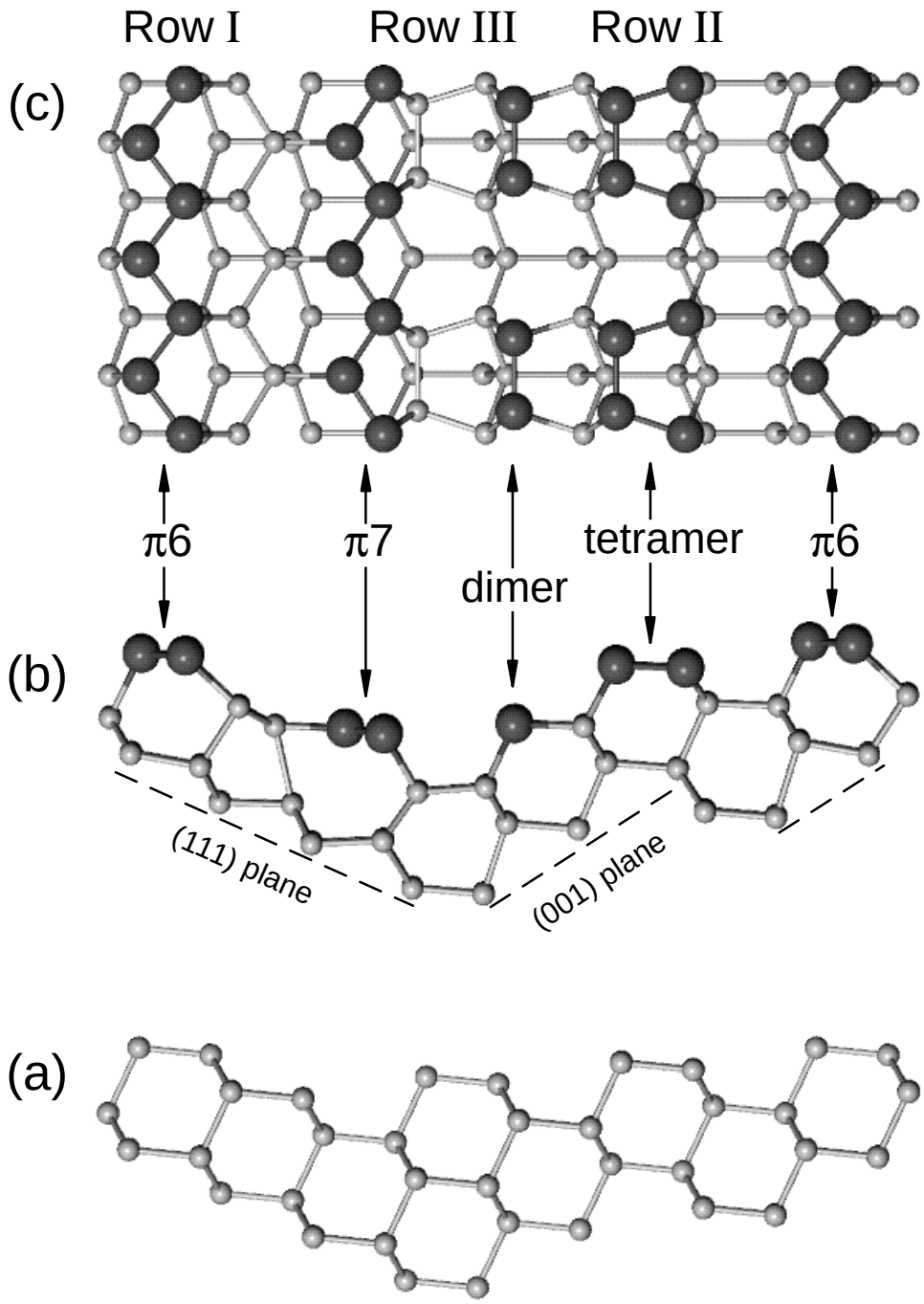

Figure 10

Baski *et al.*

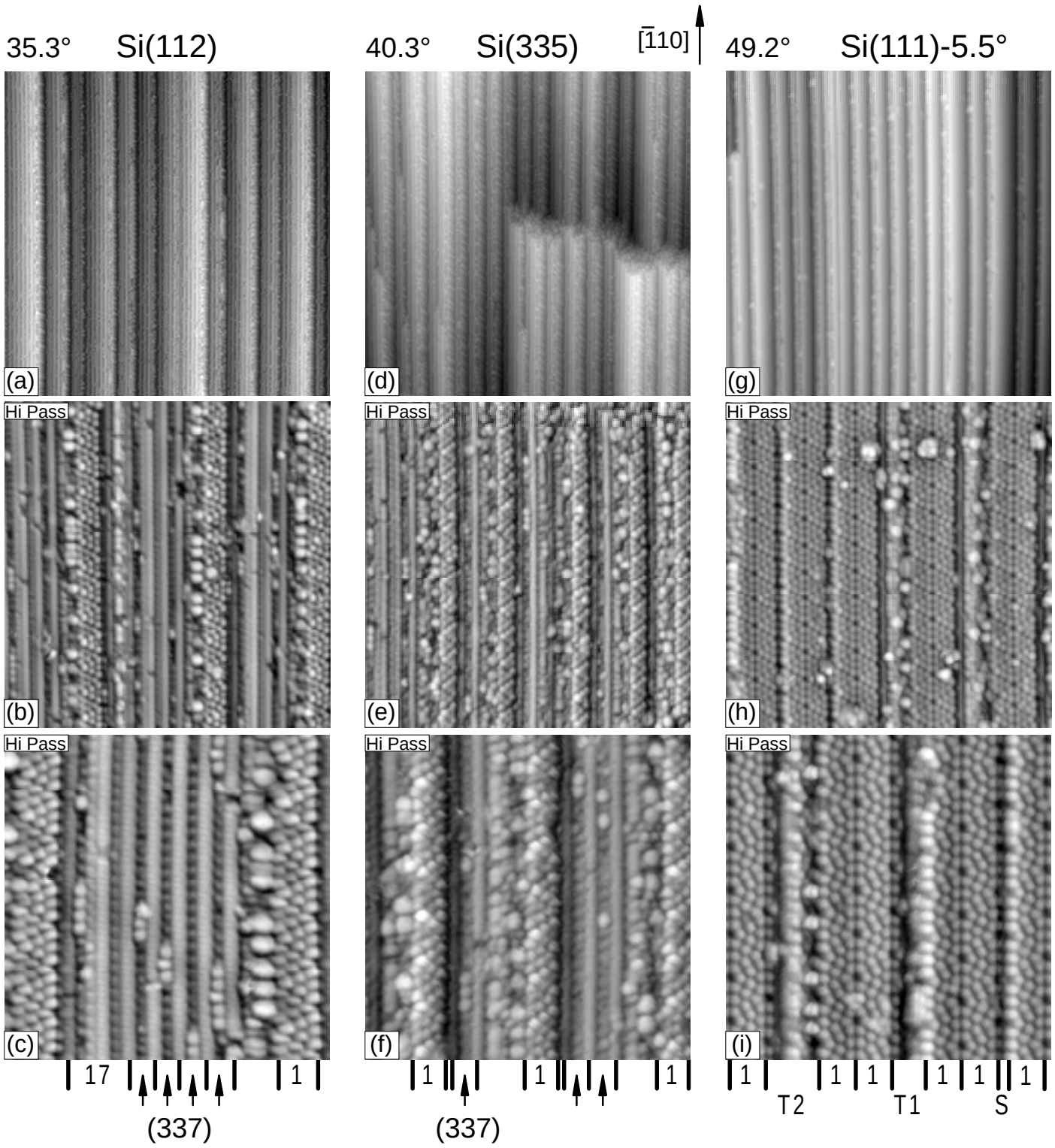

Figure 11

Baski *et al.*